Wideband Metamaterial Solar Cell Antenna for 5 GHz Wi-Fi Communication

Michael Elsdon$^{1,\,*}$, Okan Yurduseven^2, and Xuewu Dai^1

Abstract—In this paper, a novel design for a wideband integrated photovoltaic (PV) solar cell patch antenna for 5 GHz Wi-Fi communication is presented and discussed. The design consists of a slot loaded patch antenna with an array of complimentary split ring resonators (cSRR) etched in the ground plane. This is then integrated with a solar cell element placed above the patch, where the ground plane of the solar cell acts as a stacked antenna element from an RF perspective. The design is simulated on CST Microwave Studio and fabricated. The results indicate that an impedance bandwidth of 1 GHz is achieved to cover the 5 GHz Wi-Fi band with a directive gain of between 7.73 dBi and 8.18 dBi across this band. It is also demonstrated that size reduction of up to 25% can be achieved. Moreover, it is noted that using a metamaterial loaded ground plane acts as an impedance transformer, therefore the antenna can be fed directly with a 50 Ω microstrip feed line, hence further reducing the overall size.

1. INTRODUCTION

The green communication concept of using wireless communications powered from photovoltaic (PV) sources is attractive. However, in applications where device size is important, the PV cells and antennas will compete for the available surface space, as the PV power generator and the radio frequency (RF) antenna are two separate systems working at different electromagnetic bands for different purposes. Integrating the RF antenna with the PV cell into one device is desired, which will not only provide an energy-saving solution to the green wireless communication, but also substantially reduce the size and weight of communication devices and lead to new cost-effective product design. At present, these two systems are optimized for their own functions and performances, (e.g., power generation, solar conversion efficiency, fill factor, temperature, output resistance of PV cells, and impedance matching, bandwidth, beamwidth of RF antenna). The challenge is how the performances of individual systems are maintained when they are integrated into one device. Furthermore, 5 GHz wireless communication is a quickly emerging technology that is becoming popular over the long existing 2.4 GHz technology, but the 5 GHz wideband solar cell antenna design is still a challenge [1]. Operating at 5 GHz offers advantages over 2.4 GHz in terms of number of channels, interference and throughput. The 2.4 GHz band used by the IEEE 802.11b/g/n is congested with only three non-overlapping channels and commonly shared by other communication networks and home/medicine appliances (e.g., Bluetooth, microwave ovens), which results in higher interference. 5 GHz Wi-Fi has 23 non-overlapping channels and recent 802.11ac for 5 GHz Wi-Fi implements many newer technologies, such as MU-MIMO, beamforming etc., to achieve much higher throughput at shorter distance.

At 5 GHz the bandwidth has been extended to 700 MHz (5180–5825 MHz) in comparison to 94 MHz (2401–2495 MHz) for 2.4 GHz operation and the design of photovoltaic antennas are challenged by the wideband requirement for 5 GHz operation. There has been some work on solar cell integrated antennas,

* Corresponding author: Michael Elsdon (michael.elsdon@northumbria.ac.uk).
^{1} Department of Physics and Electrical Engineering, Northumbria University, Newcastle upon Tyne, NE1 8ST, UK. ^{2} Department of Electrical and Computer Engineering, Duke University, Durham, 27708, North Carolina, USA.

however most of them are designed for narrow band applications. A previous effort was done by [2], who designed an antenna array integrated with multi crystalline silicon solar cell for use in wireless sensor at 2.45 GHz. A slot antenna integrated with commercial photovoltaic (PV) panels was proposed in [3] for GSM/UMTS (1710–2170 MHz) and WiMAX (3300–3800 MHz) frequency bands. In [4], a reflectarray antenna integrated with solar cells was designed for Ka-band (26.5–40 GHz) satellite communications. In [5], an optically transparent reflect array antenna integrated with solar cells for operation at Ku band was proposed.

As previously mentioned, one of the key requirements for mobile devices is the size constraint. In view of this, the microstrip antenna is an established form of antenna that has found use in a number of personal communication applications including GPS, paging, wireless computing links, remote control, mobile phones, etc.. The advantages of microstrip antennas such as their low-profile, light weight and conformability are widely known. Conversely, one of the major disadvantages of these antennas is their inherently narrow bandwidth. The relationship between antenna size and bandwidth is well known. As the antenna size reduces, this typically results in a reduced bandwidth or reduction in efficiency. This would suggest that patch antennas in their basic form are unsuitable for 5G Wi-Fi operation. Techniques for increasing the bandwidth include the use of slot loading, stacked patch configuration, fractal geometry and more recently the use of metamaterials.

Metamaterials were first proposed by [6]. These are artificially created homogenous materials exhibiting unusual dielectric characteristics that can be engineered and are not available in nature. The use of metamaterials in antenna design has received considerable attention in recent years. One of the major reasons for this is the ability to create double-negative (DNG) materials with a simultaneous ε-negative and μ-negative responses as demonstrated by Smith et al. in 2000 [7]. In recent years, several studies have been published which use metamaterials to increase the antenna bandwidth. These include loading the radiating element of a patch with complementary split-ring resonator (cSRR) [8], employing a metamaterial superstrate [9] or using cSRR in the ground plane [10].

A further consideration for future mobile devices is the ability to be self-powered by the use of solar cell technology. In view of this and also the size limitation of future mobile devices, a number of designs for fully integrated photovoltaic antennas have been reported [11–18]. These can be broadly categorized into three main design types; including the use of solar cells as an RF ground plane [11, 12], as an RF radiating element [13] and as an RF stacked parasitic patch element suspended above the radiating element [14, 15]. A key factor when designing such antennas is the trade-off between RF performance and solar efficiency. The first involves using the solar cell as an RF ground plane [11, 12]. The major disadvantage of this technique is the reduced solar efficiency due to the shading effect of the antenna structure. Two possible approaches to reduce this effect include either meshing the antenna element [11, 12] or using transparent conductive antennas [13–15]. It has been reported that using transparent conductive antennas allows only 75% visible light transmission and moreover a radiation efficiency of 50% has been reported [14]. Conversely, it has been demonstrated that the use of meshed elements allows visible light transmission of up to 80%. A further consideration for this technique is the limited freedom to optimize the antenna structure to modify the RF response to achieve wideband performance. The second approach involves using the solar cells as an RF radiating element [16, 17]. This approach eliminates the shading problem, however it allows little freedom to modify the RF response of the element due to the fact that the solar cells need to be homogeneous in structure to achieve optimum solar efficiency. The third technique involves the use of solar cells as a stacked element suspended above the radiating element [18]. Using this approach eliminates the shading problem and moreover from an RF viewpoint allows modification of the antenna structure without effecting the solar performance. This structure also allows a number of degrees of freedom to optimize the antenna performance.

In summary, the three key requirements for antennas operating across the 5 GHz Wi-Fi band are size, bandwidth and the ability to be self-powered. In this paper, a new design using a slot loaded patch antenna with an array of complementary split-ring resonator (cSRR) etched in the ground plane, and stacked with a solar cell is presented and discussed. This design allows the antenna to cover the entire spectrum of the 5 GHz Wi-Fi band. It also simultaneously reduces the size of the antenna and achieves input impedance of 50 Ω across the entire frequency band, therefore eliminating the need for an additional impedance matching network, thus further reducing the overall size of the antenna. The proposed antenna achieves a total size reduction of 25% when compared to a standard rectangular

patch and operates over 1 GHz bandwidth. The remainder of the paper is organised as follows. Section 2 provides a description of the design procedure outlining three different designs with simulated results of antenna performance of each design. Section 3 provides experimental results while Section 4 provides concluding remarks.

2. DESIGN

In this section, three different antenna designs are presented, and their performance in terms of reflection coefficient, bandwidth, gain and size reduction are discussed.

2.1. Design of Reduced Size Antenna with Array of CSRRs in Ground Plane

The new design is illustrated in Fig. 1. It consists of a slot-loaded rectangular microstrip patch, this is fabricated on FR4-PCB, with dielectric constant of $\varepsilon_r = 4.5$ and loss tangent of $\tan\delta = 0.02$. This is placed beneath a polycrystalline (poly-Si) solar cell at a distance of 3 mm, with the ground plane (bottom contact) of the solar cell acting as a stacked element from an RF view-point. As depicted in Fig. 1(b), the solar cell consists of three layers. The first layer is the top grid contact while the second layer is the bottom contact. Both of these layers are aluminum and have a thickness of 35 µm. Between these two layers, a silicon layer is present with a thickness of 0.21 mm [12]. The electrical properties of the solar cell (open-circuit voltage, V_{op}, and short-circuit current, I_{SC}) can be found in [12, 18].

The ground plane of the solar cell is the same dimensions as the patch antenna. A top view of the slot loaded antenna is shown in Fig. 1(a) and a side view of the entire design is shown in Fig. 1(b). An array of cSRR unit cells were embedded in the ground plane of the antenna, as is illustrated in Fig. 1(c). A photo of the practical design is shown in Fig. 1(d).
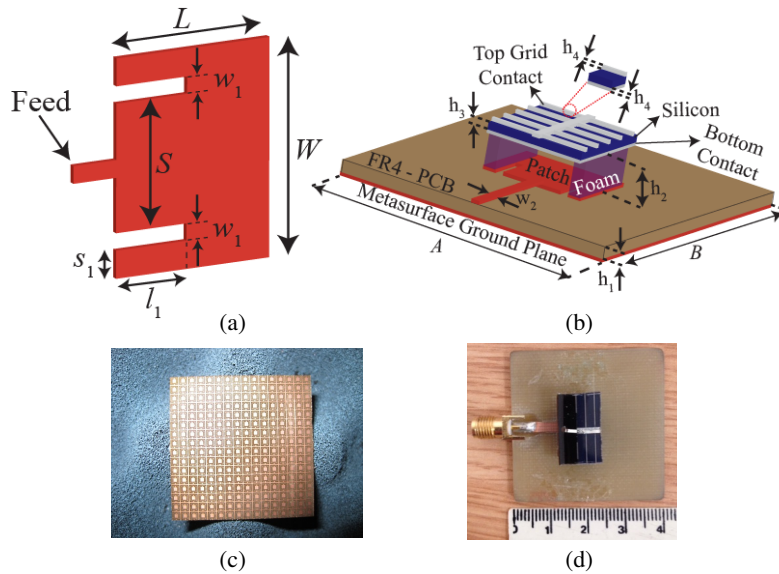

Figure 1. Patch antenna with array of cSRR in ground plane, (a) patch structure, (b) perspective view, (c) metamaterial ground plane, (d) practical design ($L = 9.8$ mm, $W = 16$ mm, $A = 40$ mm, $B = 40$ mm, $w_1 = 1$ mm, $w_2 = 2.7$ mm, $s_1 = 2$ mm, $l_1 = 6.4$ mm, $s = 10$ mm, $h_1 = 1.57$ mm, $h_2 = 3$ mm, $h_3 = 0.21$ mm, $h_4 = 35$ µm). Not drawn to scale.

The design process is outlined below. The initial stage was to determine the correct dimensions for a single unit cSRR cell (shown in Fig. 2) to obtain a negative epsilon response at the centre frequency of the 5 GHz Wi-Fi band, as shown in Fig. 3. The dimensions were achieved by simulating a single unit cell and exciting it with a plane wave.

Results of reflection (S_{11}) and transmission (S_{21}) coefficients for a single cSRR unit cell were obtained using CST software, and are shown in Fig. 3. The retrieved epsilon response is shown in
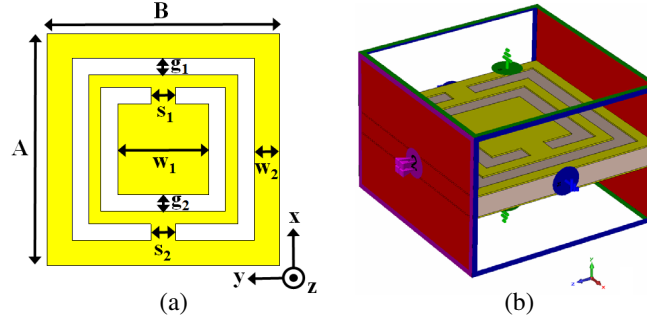
Figure 2. Ground plane cSRR unit cell (a) depiction of the cell (b) simulation setup in CST Microwave Studio (green arrow is for $\mathbf{E}_t = 0$ boundary condition and blue arrow is for $\mathbf{H}_t = 0$ boundary condition. Excitation ports are shown in red color). $A = 2.5\,\text{mm}$, $B = 2.5\,\text{mm}$, $g_1 = 0.2\,\text{mm}$, $g_2 = 0.2\,\text{mm}$, $s_1 = 0.3\,\text{mm}$, $s_2 = 0.3\,\text{mm}$, $w_1 = 1.1\,\text{mm}$, $w_2 = 0.2\,\text{mm}$.
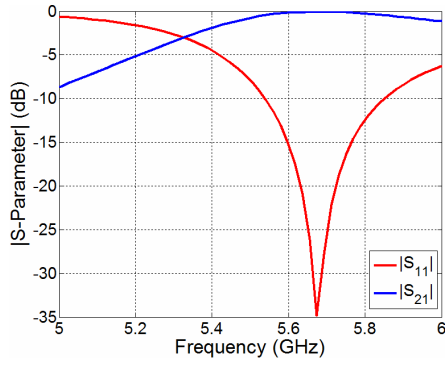

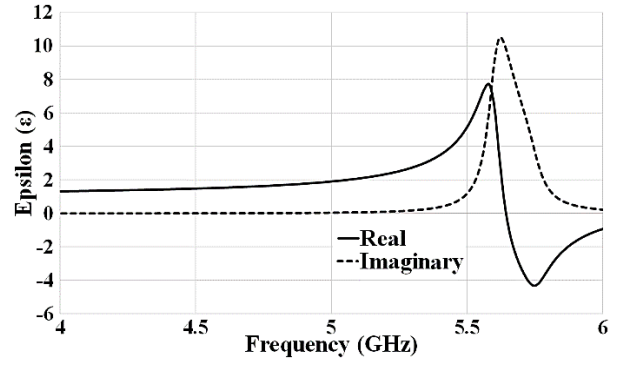**Figure 3.** S_{11} and S_{21} results for single unit cell.

Figure 4. Retrieved ε-response of the cSRR unit cell.

Fig. 4, which indicates that a negative-epsilon response is observed at 5.6 GHz.

Using this as a basis for the antenna design, the design was a three stage process. Each stage is outlined below, with all three designs simulated using CST full-wave simulation, Fig. 5(a) illustrates the real and imaginary input impedance, Fig. 5(b) illustrates the reflection coefficient for each design, Fig. 6 shows the directive gain for each design together with the radiation efficiency of the final design, Fig. 7 shows the radiation plots, whilst Table 1 summarises the antenna performance in terms of beamwidth, VSWR bandwidth, gain and size reduction. The reflection coefficient and input impedance are simulated between 4.8–6 GHz, whilst the far-field response is shown at 5.18 GHz, 5.4 GHz and 5.8 GHz to cover the entire 5 GHz Wi-Fi band.

For comparison purposes, the results of a reference antenna designed to operate at a centre frequency of 5.6 GHz, are also included. The reference antenna consists of standard rectangular patch antenna, with length $L = 12.8\,\text{mm}$ and $W = 16\,\text{mm}$, fabricated on FR4 PCB with a permittivity of 4.5 and thickness 1.57 mm. Impedance matching was achieved using a quarter-wave matching network. A solid ground plane was also used.

2.2. Design 1: Regular Patch Antenna with Metamaterial Ground Plane

The second stage in the design process was to model a standard rectangular patch, fabricated on FR4-PCB with an array of cSRR etched in the ground plane. In this example, a standard rectangular patch with a centre frequency of 5.6 GHz was chosen. Patch dimensions, $L = 10.5\,\text{mm}$ and $W = 16\,\text{mm}$, were determined using CST simulations. An array of cSRR elements are etched on the ground plane of the antenna, with dimensions determined as in Figs. 1 and 2. For this design a negative-epsilon response is achieved, which accounts for the size reduction.
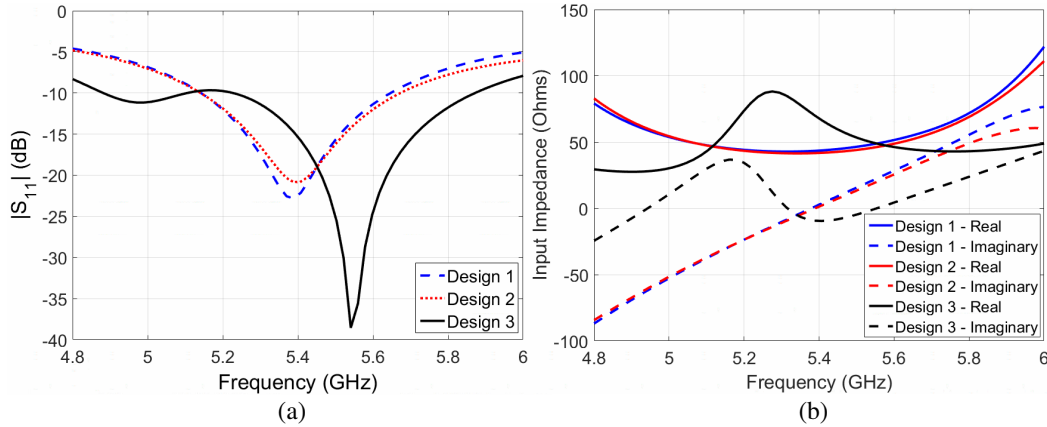
Figure 5. Simulated reflection and impedance patterns of designs 1, 2 and 3 (a) $|S_{11}|$ response (b) real and imaginary input impedance.
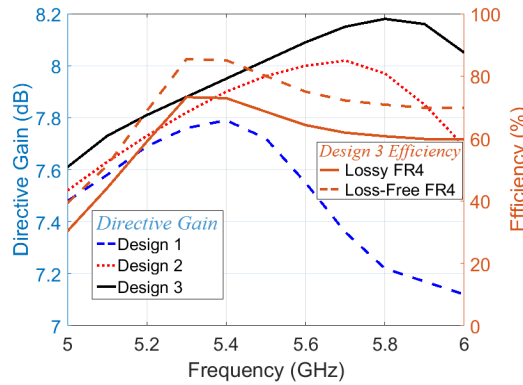

Figure 6. Directive gain responses of the designs 1, 2 and 3 and efficiency of design 3 (with and without the loss of the FR4 substrate).

The S_{11} pattern, illustrated in Fig. 5(a) (dashed blue line), indicates a good impedance match at 5.6 GHz. Plots of real and imaginary impedance are illustrated in Fig. 5(b). As shown in Fig. 5(b), the real input impedance is maintained between $Z_{in}(\text{real}) = 41\,\Omega$ and $Z_{in}(\text{real}) = 71\,\Omega$ while the imaginary input impedance is maintained between $Z_{in}(\text{im}) = -j27\,\Omega$ and $Z_{in}(\text{im}) = j55\,\Omega$ across the 5 GHz Wi-Fi band.

The results also indicate that the metamaterial in the ground plane increases the bandwidth to a 500 MHz, however this is not sufficient to fully cover the 700 MHz bandwidth required for 5 GHz Wi-Fi. Examining Fig. 6 demonstrates a reduction in directive gain with frequency. Examining Fig. 7, it can be seen that broadside radiation is achieved for Phi = 90°, with slightly off axis radiation is achieved for Phi = 0°. Table 1 illustrates a 3 dB beamwidth of 70° at 5.6 GHz.

2.3. Design 2: Stacked Solar Cell Element with Metamaterial Ground Plane

The next stage in the design process is to introduce the solar element. This is achieved by using the ground plane of a solar cell element acting as a suspended RF element. Patch dimensions, $L = 10.5\,\text{mm}$ and $W = 16\,\text{mm}$, remained the same as design 1. It is found that placing this at a distance of 3 mm above the lower patch further increases the bandwidth to 600 MHz, as illustrated in Fig. 5(b) (dotted red line). The S_{11} pattern, illustrated in Fig. 5(a) (dashed blue line), indicates a good impedance match at 5.6 GHz. Plots of real and imaginary impedance are illustrated in Fig. 5(b). It can be seen that the real input impedance remains between $Z_{in}(\text{real}) = 40\,\Omega$ and $Z_{in}(\text{real}) = 69\,\Omega$ while the imaginary input impedance is maintained between $Z_{in}(\text{im}) = -j27\,\Omega$ and $Z_{in}(\text{im}) = j48\,\Omega$ across the 5 GHz Wi-Fi band.
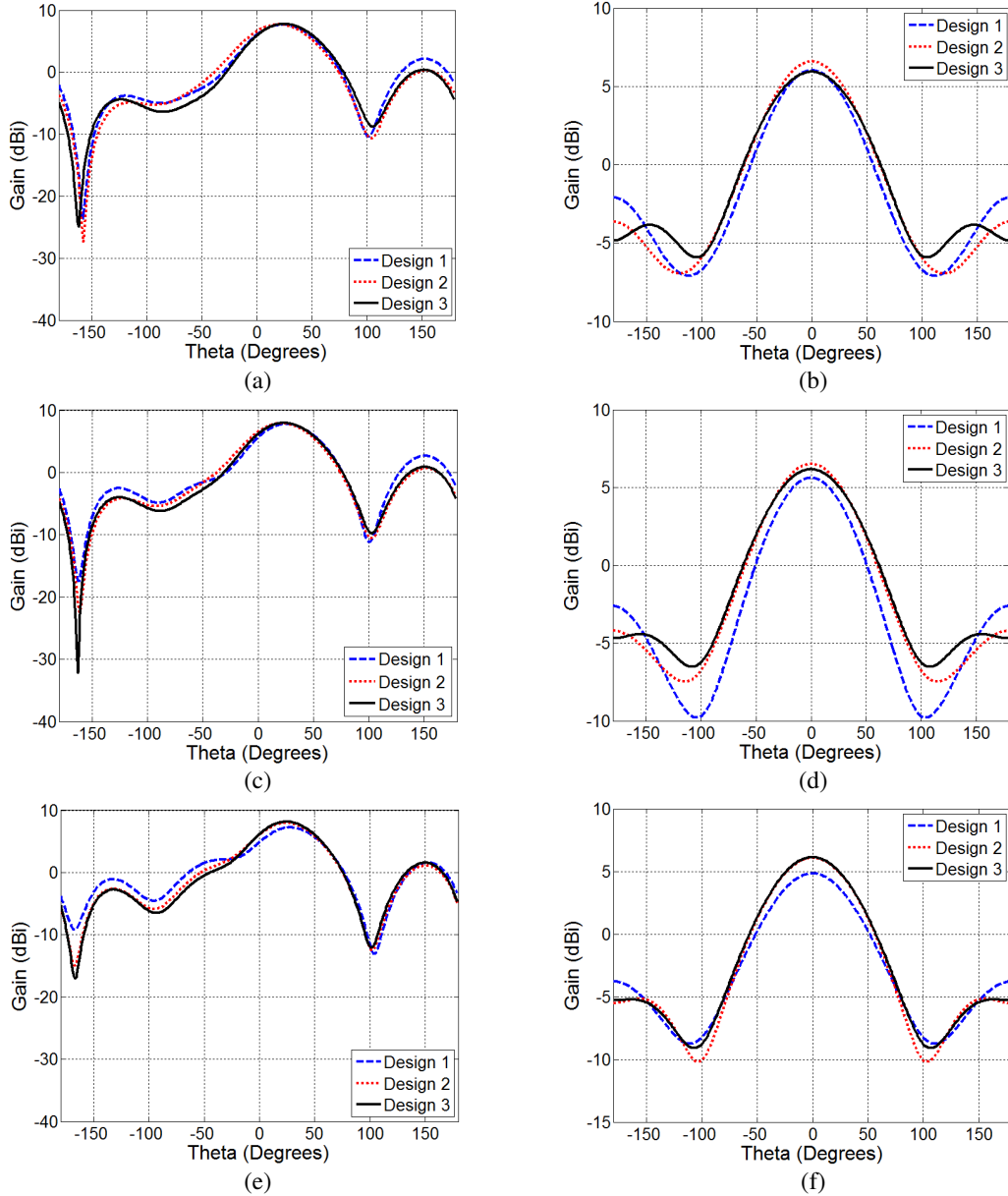
Figure 7. Radiation plots of gain vs. angle for designs 1, 2 and 3 at different frequencies; (a) frequency = 5.18 GHz, phi = 0°, (b) frequency = 5.18 GHz, phi = 90°, (c) frequency = 5.4 GHz, phi = 0°, (d) frequency = 5.4 GHz, phi = 90°, (e) frequency = 5.8 GHz, phi = 0°, (f) frequency = 5.8 GHz, phi = 90°.

Examining Fig. 6 demonstrates a higher directive gain compared to design 1 with a slight decrease in directive gain with frequency. Examining Fig. 7, it can be seen that broadside radiation is achieved for Phi = 90°, while the radiation for Phi = 0° is observed to be slightly off axis. It is also noted from Table 1 that a beamwidth of 78° is achieved at 5.6 GHz.

2.4. Design 3: Slot Loaded of Patch with Stacked Solar Element and Metamaterial Ground Plane

To fully cover the 700 MHz bandwidth required for 5 GHz Wi-Fi, slot loading was introduced. This has the effect of producing an additional $TM_{0\delta}$ resonance mode to further increase the bandwidth. The slot

Table 1. Performance of proposed antenna designs.

	Patch Length, mm	Size Reduction (%)	VSWR Bandwidth	Directive Gain (5.6 GHz)	Realized Gain (5.6 GHz)	Beam width
Reference Antenna	12.8	N/A	0.152 GHz	7.21 dBi	3.78 dB	79°
Design 1	10.5	20	0.5 GHz	7.79 dBi	2.73 dB	70°
Design 2	10.5	20	0.6 GHz	7.9 dBi	3.55 dB	78°
Design 3	9.8	25	1.05 GHz	7.95 dBi	4.14 dB	83°

also reduces the current path for the TM_{01} mode hence accounting for an increase in resonant frequency of this mode. The S_{11} pattern, shown in Fig. 5(a) (solid black line), demonstrate a -10 dB bandwidth of 1 GHz. Examining Fig. 6 demonstrates a slight decrease in directive gain compared to design 3 in the lower half of the band, however directive gain is still relatively constant ranging from 7.73 dBi to 8.18 dBi across the 5 GHz Wi-Fi band. The radiation efficiency of design 3 is also plotted in Fig. 6 as a function of the operating frequency band. Analyzing Fig. 6, it can be concluded that the loss of the FR4 substrate has a considerable effect on the radiation efficiency of the antenna. Examining Fig. 7, it can be seen that broadside radiation is achieved for Phi $= 90°$, with slightly off axis radiation is observed for Phi $= 0°$. It is also noted, from Table 1, that the 3 dB beamwidth increases to 78° at 5.6 GHz.

A typical trade-off from regular patch antenna with slot loading is an increase in input impedance at the patch periphery, which causes problems regarding impedance matching. Traditional techniques for exciting a patch antenna include the use of quarter-wave matching, probe-feed, aperture coupling and proximity coupling. These matching techniques all add to the overall size or complexity of the antenna. Examining plots of real and imaginary impedance, illustrated in Fig. 5(b), it can be seen that the real input impedance is maintained between $Z_{in}(\text{real}) = 40\,\Omega$ and $Z_{in}(\text{real}) = 87\,\Omega$ while the imaginary input impedance is within the range of $Z_{in}(\text{im}) = -j10\,\Omega$ and $Z_{in}(\text{im}) = j36\,\Omega$ across the 5 GHz Wi-Fi band. Using the design proposed in this paper allows the input impedance to be maintained near to $50\,\Omega$, which eliminates the requirement for impedance matching.

From previous literature, although slot loading reduces the antenna size, a significant trade-off from this is a reduction in bandwidth. The results for the proposed design indicate that this is not apparent for this design.

3. RESULTS AND DISCUSSION

A prototype of the proposed design was fabricated on FR4 with a permittivity of $\varepsilon_r = 4.5$ and thickness 1.57 mm. The measured and simulated S_{11} patterns for this design are shown in Fig. 8, which demonstrates a measured return loss of 21 dB and 40 dB at 5.55 GHz. This equates to a size reduction of 25% when compared to a standard rectangular patch antenna operating at the same frequency. Both the simulated and the measured S_{11} patterns exhibit fairly good agreement in terms of the -10 dB bandwidth, with both patterns crossing the -10 dB threshold at similar frequencies in the lower and upper frequency bands. A measured $2:1$ VSWR bandwidth of 0.89 GHz from 5.2–6.1 GHz with a centre frequency of 5.6 GHz is also noted which compares to a 1.05 GHz simulated bandwidth. The simulated design exhibits 1.05 GHz bandwidth ($|S_{11}|$ remaining -10 dB across 4.85–5.9 GHz), while the measured result has 0.89 GHz bandwidth ($|S_{11}|$ remains below -10 dB across 5.2–6.1 GHz).

A plot of the measured radiation patterns in both E and H-planes is shown in Fig. 9. The proposed antenna exhibits broadside radiation with good agreement being observed with the simulated results, although the sidelobes in the E-plane are slightly higher. A realised gain of 3.94 dBi was measured at the centre frequency 5.6 GHz, which demonstrates a slight reduction when compared to the 4.14 dBi predicted results.

In summary, it can be seen there is good general agreement between simulated and measured results. There are a number of factors that account for slight variation between the two sets of results,
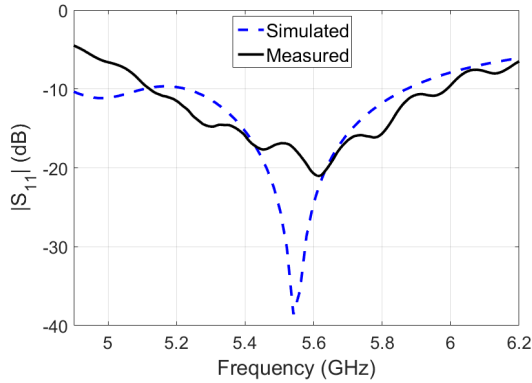
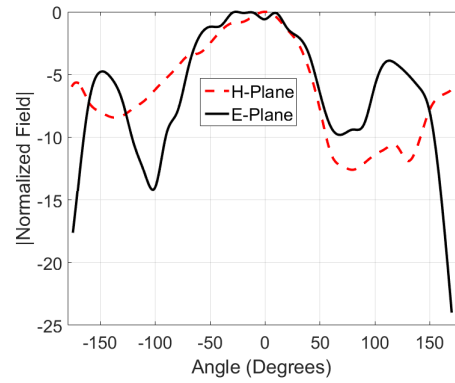**Figure 8.** S_{11} responses of the proposed design.

Figure 9. Measured normalized E-plane and H-plane far-field radiation patterns at 5.6 GHz.

such as the fabrication tolerances of the antenna (limited by the PCB printer), calibration of the vector network analyzer, the quality of the connection of the SMA port, and possible multi-reflections in the measurement environment.

4. CONCLUSION

A novel wideband integrated solar cell antenna for use in 5 GHz Wi-Fi applications has been presented and discussed. It has been demonstrated that using this design an impedance bandwidth of up to 1 GHz can be achieved whilst also achieving size reduction of up to 25% and maintaining a directive gain above 7.73 dBi over the entire Wi-Fi spectrum. The design also removes the requirement for an external impedance matching network.

REFERENCES

1. Ang, B.-K. and B.-K. Chung, "A wideband e-shaped microstrip patch antenna for 5–6 GHz wireless communications," *Progress In Electromagnetics Research*, Vol. 75, 397–407, 2007.
2. O'Conchubhair, O., P. McEvoy, and M. J. Ammann, "Integration of antenna array with multicrystalline silicon solar cell," *IEEE Antennas and Wireless Propagation Letters*, Vol. 14, 1231–1234, 2015.
3. Caso, R., A. D'Alessandro, A. Michel, and P. Nepa, "Integration of slot antennas in commercial photovoltaic panels for stand-alone communication systems," *IEEE Transactions on Antennas and Propagation*, Vol. 61, No. 1, 62–69, Jan. 2013.
4. Ang, B. K. and B.-K. Chung, "A wideband E-shaped microstrip patch antenna for 5–6 GHz wireless communications," *Progress In Electromagnetics Research*, Vol. 75, 397–407, 2007.
5. Moharram, M. A. and A. A. Kishk, "Optically transparent reflectarray antenna design integrated with solar cells," *IEEE Transactions on Antennas and Propagation*, Vol. 64, No. 5, 1700–1712, May 2016.
6. Veselago, V. G., "The electrodynamics of substances with simultaneously negative values of ε and μ," *Sov. Phys. Usp.*, Vol. 10, No. 4, 509–514, 1968.
7. Smith, D. R., W. J. Padilla, D. C. Vier, S. C. Nemat-Nasser, and S. Schultz, "Composite medium with simultaneously negative permeability and permittivity," *Physical Review Letters*, Vol. 84, No. 18, 4184–4187, 2000.
8. Raghavan, S. and V. Anoop Jayaram, "Metamaterial loaded wideband patch antenna," *PIERS Proceedings*, 760–763, Taipei, Taiwan, Mar. 25–28, 2013.

9. Ju, J., D. Kim, W. J. Lee, and J. I. Choi, "Wideband high gain antenna using metamaterial superstrate with the zero refractive index," *Microwave and Optical Technology Letters*, Vol. 51, No. 8, 1973–1976, 2009.

10. Li, L.-W., Y.-N. Li, T. S. Yeo, J. R. Mosig, and O. J. F. Martin, "A broadband and high-gain metamaterial microstrip antenna," *Applied Physics Letters*, Vol. 96, 164101, 2010.

11. Turpin, T. W. and R. Baktur, "Meshed patch antennas integrated on solar cells," *IEEE Antennas Wireless Propag. Lett.*, Vol. 8, 693–696, 2009.

12. Yurduseven, O., D. Smith, and M. Elsdon, "UWB meshed solar monopole antenna," *Electron. Lett.*, Vol. 49, No. 9, 582–584, Apr. 2013.

13. Ito, K. and M. Wu, "See-through microstrip antennas constructed on a transparent substrate," *Seventh International Conference on Antennas and Propagation*, Vol. 1, 133–136, 1991.

14. Yasin, T., R. Baktur, and C. Furse, "A study on the efficiency of transparent patch antennas designed from conductive oxide films," *IEEE International Symposium on Antennas and Propagation (APSURSI)*, 3085–3087, 2011.

15. Yurduseven, O. and D. Smith, "A solar cell stacked multi-slot quad-band PIFA for GSM, WLAN and WiMAX networks," *IEEE Microwave and Wireless Components Letters*, Vol. 23, No. 6, 285–287, Jun. 2013.

16. Danesh, M. and J. R. Long, "An autonomous wireless sensor node incorporating a solar cell antenna for energy harvesting," *IEEE Trans. Microw. Theory Tech.*, Vol. 59, No. 12, 3546–3555, Nov. 2011.

17. Vaccaro, S., J. R. Mosig, and P. de Maagt, "Making planar antennas out of solar cells," *Electron. Lett.*, Vol. 38, No. 17, 945–947, Aug. 2002.

18. Yurduseven, O., D. Smith, N. Pearsall, and I. Forbes, "A solar cell stacked slot-loaded suspended microstrip patch antenna with multiband resonance characteristics for WLAN and WiMAX systems," *Progress In Electromagnetics Research*, Vol. 142, 321–332, 2013.